Shear-lag modelling of surface-bonded magnetostrictive transducers for shear horizontal wave generation in a non-ferromagnetic plate

Fuzhen Wen[1,2,3], Shengbo Shan[1,2,3], Rafal Radecki[4], Wieslaw J. Staszewski[4] and Li Cheng[1,2,3]

[1] Department of Mechanical Engineering, The Hong Kong Polytechnic University Kowloon, Hong Kong

[2] Shenzhen Research Institute, The Hong Kong Polytechnic University, Shenzhen, China

[3] Hong Kong Branch of National Rail Transit Electrification and Automation Engineering Technology Research Center, The Hong Kong Polytechnic University, Kowloon, Hong Kong

[4] Department of Robotics and Mechatronics, AGH University of Science and Technology, Al. Mickiewicza 30, 30-059 Krakow, Poland

E-mail: li.cheng@polyu.edu.hk

Abstract

The fundamental shear horizontal wave in thin-walled structures shows appealing features for structural health monitoring applications. Its efficient generation and reception however remain a critical and challenging issue. Magnetostrictive transducers show proven ability in exciting strong shear horizontal waves due to the high piezomagnetic coefficient of the ferromagnetic foil. In this study, to investigate the fundamental shear horizontal wave generation using magnetostrictive transducers and their design, a theoretical model is

established based on the shear-lag model and the normal mode expansion method. The coupling of a magnetostrictive transducer with a host plate is achieved by a bonding layer, whose mechanical property is modelled through the continuous shear stress across the thickness. The theoretical model is validated using finite element simulations in terms of generation mechanism and some typical features associated with the fundamental shear horizontal wave component. Meanwhile, wave field is visualized using a 3-D Laser scanning vibrometer system. Experimental results within a wide frequency range show a good agreement with the theoretically predicted results. Influences of the coil configuration and bonding conditions are further investigated using the proposed model. The study offers guidelines to system design and optimization for fundamental shear horizontal wave generation in views of guided-wave-based structural health monitoring applications.

Keywords: Structural Health Monitoring, Fundamental Shear Horizontal Wave, Magnetostriction, 3-D Laser, Frequency Tuning Curve

1 Introduction

Guided waves offer appealing properties for structural health monitoring (SHM) applications due to their long travelling distance with low energy loss [1-3]. Among various guided wave modes, the fundamental shear horizontal (SH0) waves show high potential for the detection of structural defects owing to several appealing features [4-6]. Firstly, SH0 wave mode is non-dispersive, namely the shape of a wave packet remains unchanged during the propagation in a homogenous medium [7-8]. Secondly, particle motion in SH waves is restricted to the in-plane layer [9], thus offering immunity to energy leakage into the surrounding liquid environment. Thirdly, when SH0 wave is reflected from a surface

parallel to the direction of polarization, no mode conversion occurs. These advantages are conducive to SHM implementation and facilitate the interpretation of the captured response signals for damage detection.

Successful implementation of SH0-wave-based SHM strongly relies on the proper design of the detection system, with the foremost requirement for effective wave generation and reception [3]. Well-known wave generation techniques include methods based on piezoelectric transducers or electromagnetic transducers. Piezoelectric wafer-type shear transducers [10-11] have shown proven efficiency and cost-effectiveness for SH0 wave generation and reception with different working modes, *i.e.* d_{15} [9], d_{35} [2,10], d_{24} [12,13] and d_{36} [4,14,15]. However, their capabilities for SH0 wave excitation are highly dependent on the size of the piezoelectric transducers and less effective for high-frequency applications. In contrast, Electro-Magnetic Acoustic Transducers (EMATs) attract increasing attentions due to the flexibility they offer in choosing excitation frequencies through proper coil design [16]. The operation of the EMATs involves three mechanisms via the coupling between the electromagnetic field and the elastic field as (i) the Lorentz force caused by the interaction between the eddy current and the static magnetic flux density, (ii) the magnetization force between the oscillating magnetic field and the magnetizations, and (iii) the magnetostrictive mechanism by the piezomagnetic effect [17]. In non-ferromagnetic conductive materials, the induced Lorentz force directly excites SH0 waves. By contrast, in ferromagnetic materials, the magnetostriction is usually the dominant mechanism behind SH wave generation when the static field is parallel to the sample surface. In contrast to the Lorentz force effect, the magnetostriction is dependent not only on the excitation current but also on the piezomagnetic coefficients of the material.

The requirement for strong SH0 wave generation leads to the deployment of the so-called Magnetostrictive Transducers (MsTs). MsTs operating in accordance with the magnetostrictive principle have been used to generate and measure ultrasonic waves at frequencies ranging from roughly 20 kHz to 2 MHz, in various waveguides such as pipes and plates [18-21]. The basic configuration of a typical MsT contains three components: a permanent magnet to supply a bias static magnetic field, an AC-current coil to provide a dynamic magnetic field and a magnetostrictive patch with high piezomagnetic coefficients to generate shear strains in response to an applied magnetic field. The deployment of strong adhesives–like epoxy resin glues–ensures highly efficient strain transfer when the patch is properly surface-bonded on the host structure. With such a premise, MsT-induced SH0 waves can be used for damage detections in non-ferromagnetic systems such as aluminum or composite plates.

The performance of MsTs is highly dependent on various parameters, including the configuration of the coil, the magnetostrictive patch, bonding layers and their material properties and so on. Therefore, system modelling is vital to simulate the wave generation and propagation process to guide the choice of various system parameters and eventually the optimization of the SHM systems. Thompson *et al*. developed a general analytical framework covering both Lorentz force and magnetostrictive coupling mechanisms [22,23]. Inspired by their work, the design of magnetostrictive transducers were extensively investigated by Ogi *et al.* [24]. Furthermore, a model for the coupling between the elastic and magnetic fields was proposed to study the magnetostriction body forces generated in a ferromagnetic material [25]. Based on that, SH guided waves in a ferromagnetic plate induced by the magnetostrictive effect were explored in [16, 26]. Most existing models

mainly focus on the shear wave generation in ferromagnetic materials where the excitation force induced by the electro-magnetic field directly applies on the waveguide. For non-ferromagnetic materials/structures, however, a magnetostrictive patch is indispensable which allows for the transfer of the electro-magnetic field-induced excitation force to the waveguide through an adhesive layer. Efforts [8,27-29] have been made on the investigations of guided wave generation in non-ferromagnetic plates using magnetostrictive patch transducers (MPTs), which share similar configuration with the MsT used in the present study. More specifically, Kim *et al*. [30] proposed an equivalent source model to study the SH wave generation problem by MsT. Through finite element model, analyses of the dynamic magnetic field generated by the coil and the development of the corresponding equivalent excitation source were performed. The bonding conditions of the MsT patch, however, was not the focus in that work. Therefore, a theoretical model capable of characterizing the SH wave generation with an MsT through an adhesive layer is required. Meanwhile the model is expected to offer enhanced wave prediction efficiency and to provide design guidelines of MsT-activated SHM system, which motivates the present work.

To tackle this problem, a systematic investigation on the SH0 wave generation in an MsT-activated SHM system–containing an adhesive layer–is conducted in this paper. A theoretical model is formulated by considering a magnetostrictive patch bonded on a plate through an adhesive layer. The shear-lag model developed by Giurgiutu *et al.* is extended to solve the SH wave excitation problem [31,32]. Meanwhile, the wave propagation is solved by the normal mode expansion (NME) method. The accuracy of the model is first assessed through finite element (FE) validation using typical cases in both time- and

frequency-domains. Experiments are then carried out for further validations and phenomenon verifications. Additionally, the captured Lamb waves in the host plate are also discussed to better justify the experimental results. With the proposed theoretical model, guidelines for the MsT system design are presented, through investigating the meander-line coil configuration and the bonding layer conditions. Finally, the last section renders concluding remarks.

2 Theoretical model

A typical 2-D MsT-based SH0 wave generation model, as sketched in figure 1, is investigated. The meander-line coil above the magnetostrictive patch is depicted by cross-sections, in which the red points and blue crosses denote the alternating current with inverse current directions in the adjacent segments of the coil. Specifically, the coil configuration is defined by two parameters, *i.e.*, the periodicity distance D and the fold number N_f as depicted in figure 1. D describes the distance between two coil segments in which the currents propagate along the same direction. N_f denotes the number of the coil unit, each containing two adjacent segments of the coil. The length of the MsT is $N_f \times D = 2a$. The dynamic magnetic field surrounding the coil is produced by the current, being perpendicular to a static magnetic field induced by a permanent magnet. Based on the Wiedemann effect of the magnetostriction principle, shear deformation is generated in the ferromagnetic material in response to the magnetic field, giving rise to SH0 waves [33].

Three basic elements are considered in the theoretical model. Firstly, a closed-form solution for the magnetic field in the magnetostrictive patch is given by accounting for the

periodicity of the meander-line coil. The excitation shear strain is obtained through the analysis of the coupling equations between the elastic and magnetic fields. After that, the transformation from the shear strain to the surface stress between the bonding layer and the metal plate is modeled by the classical shear-lag method. Finally, the NME framework is introduced to describe the SH0 mode waves generated by the surface stress. Modal participation factors are used to predict the frequency-domain features. With a convolution integral, the time-domain amplitudes (either strain or displacement) of the SH0 waves in the MsT-activated system are eventually obtained. In what follows, all these modelling elements are described in detail.

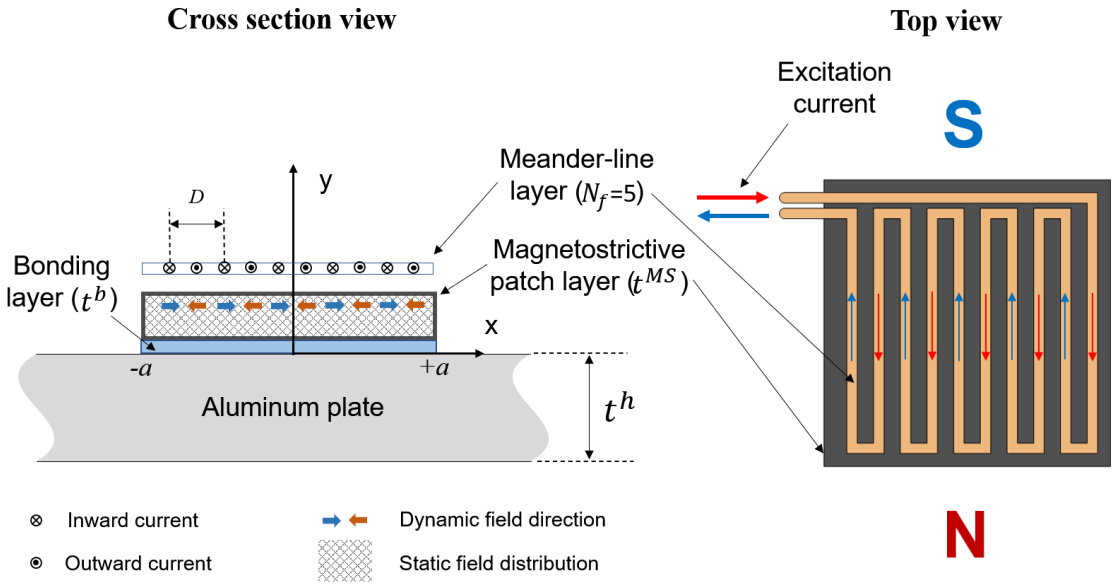

Figure 1. Sketch of the wave generation model.

2.1 Excitation shear strain in magnetostriction patch

Consider an alternating current passing through the coil along *z* direction. The calculation of the magnetic field is restricted to the *x*-*y* plane. Prior to equation derivations, several commonly used approximations are introduced to simplify the analyses. First, the influence

of the skin effect and that of the proximity effect on the coil conductor are ignored [26]. Second, the time-dependency of the displacement current density $\partial D/\partial t$ in Maxwell's equations is neglected. The frequency range of interest (50 kHz to 500 kHz in this work) in a typical MsT application is relatively lower than 20 MHz. Under such condition, the current displacement can be considered as permanent compared to particle displacement. Third, due to the relatively weak dynamic magnetic field, a linear approximation of the magnetostrictive relation is imposed, in a way similar to many previous studies [18,20,21]. In addition, eddy current effects in the magnetostrictive patch are deemed negligible, since the frequency range under investigation is relatively low [20,21]. Finally, the volume of the ferromagnetic metal does not change during the magnetostriction process. In the derivations, the time harmonic term $e^{j\omega t}$ is omitted for brevity. Following these assumptions [33], Maxwell's equations with Ampere's law and Faraday's law write

$$\frac{\partial H_x}{\partial y} - \frac{\partial H_y}{\partial x} = J_z, \tag{1}$$

$$\frac{\partial E_z}{\partial x} = -\mu_0 \bar{\mu} \frac{\partial H_y}{\partial t}, \tag{2a}$$

$$\frac{\partial E_z}{\partial y} = \mu_0 \bar{\mu} \frac{\partial H_x}{\partial t}, \tag{2b}$$

where H_x and H_y denote the magnetic field along *x* and *y* directions, receptively; J_z the current density; E_z the electric field; μ_0 and $\bar{\mu}$ the free-space permeability and dimensionless relative magnetic permeability, respectively. With Ohm's law

$$J_z = \eta E_z, \tag{3}$$

one gets the following governing equations

$$\frac{\partial H_x}{\partial x} = -\frac{\partial H_y}{\partial y}, \tag{4}$$

$$\left(\frac{\partial^2}{\partial x^2} + \frac{\partial^2}{\partial y^2}\right) H_x - j\omega\eta\mu_0\bar{\mu}H_x = 0, \tag{5}$$

where η is the electrical conductivity. The two-dimensional solutions to Eqs. (4)-(5) take the form [34]

$$\begin{cases} H_x = \dfrac{2I}{\pi a}\sin\left(\dfrac{\pi w}{D}\right)e^{-2\pi h/D}e^{qy}\sin\left(\dfrac{2\pi}{D}x\right) \\ H_y = \dfrac{\sqrt{2}\pi\delta}{D}\cdot\dfrac{2I}{\pi a}\sin\left(\dfrac{\pi w}{D}\right)e^{-2\pi h/D}e^{qy}\cos\left(\dfrac{2\pi}{D}x\right) \end{cases}, \tag{6}$$

where *I* denotes the current flowing in the coil; a the half width of the patch and *h* the lift-off, namely the thickness of the air layer between the meander-line coil and the magnetostrictive patch. *D* and *w* denote the periodicity distance and the width of the meander-line wire. $\delta = \sqrt{2/\omega\eta\mu_0\bar{\mu}}$ is defined as the electromagnetic skin depth and $q \equiv -(1/\delta)(1+j)$. Eq. (6) leads to the following observations:

1. The module of the *x*-direction magnetic field H_x overwhelms that of the *y*-direction magnetic field H_y since $(2\pi\delta/D) \ll 1$.
2. The magnitude of the magnetic field exponentially decreases as the thickness of the air layer, *h*, increases.
3. The presence of the term e^{qy} leads to a drastic magnetic field impairment along with the penetration depth in the magnetostrictive patch.

The piezomagnetic coupling equations between elastic field and magnetic field write [15]

$$\begin{cases} \mathbf{S}_D = \mathbf{C}\mathbf{T}_D + \mathbf{d}^T\mathbf{H}_D \\ \mathbf{B}_D = \mathbf{d}\mathbf{T}_D + \boldsymbol{\mu}\mathbf{H}_D \end{cases}, \tag{7}$$

where **S** denotes the engineering strain tensor; **T** the stress tensor; **H** the magnetic field; **C** the compliance matrix; **d** the piezomagnetic strain coefficient and **B** the magnetic flux density. The quantities with the subscript *D* are related to the applied dynamic magnetic field induced by the meander-line coils. In this case, two components of $\mathbf{H}_D$ can be found in Eq. (6). A static uniform bias field $\mathbf{H}_S$ is applied along the *z* direction, as shown in figure 1. The effect of $\mathbf{H}_S$ on the system is considered in the coupling coefficient **d** which takes the matrix form as [35,36]

$$\mathbf{d} = \begin{bmatrix} 0 & 0 & 0 & 0 & d_{5x} & 0 \\ 0 & 0 & 0 & d_{4y} & 0 & 0 \\ d_{3x} & d_{3y} & d_{3z} & 0 & 0 & 0 \end{bmatrix}. \tag{8}$$

Substituting the solution of H_x and the coupling coefficient matrix (8) into Eq. (7) yields the transducer's strain ε_{ISA} induced by the applied magnetic field H_x, expressed as

$$\varepsilon_{ISA} = \varepsilon_{zx} = d_{5x}H_x. \tag{9}$$

2.2 Wave generation

Based on the classical shear-lag model [1], the connection between the transducer and the host structure is characterized by the interfacial shear stress in the bonding layer. The shear stress intensity and its distribution depend on the relative deformation of the transducer and

the host structure. Two assumptions are adopted, namely, (i) inertial terms of the magnetostrictive patch, bonding layer and the metal plate are neglected; (ii) the deformation of the bonding layer is simplified as pure shearing. The shear-lag model is established by formulating the governing equations that include constitutive, geometric and equilibrium equations of the actuator, the bonding layer and the host structure, respectively. The initial assumption is that the SH wave generates the particle motion along the *z*-axis, whereas the wave propagation takes place along the *x*-axis. Therefore, the displacement components of vector **u** of SH0 waves can be expressed as

$$\mathbf{u} = \left[u_x \;\; u_y \;\; u_z \right]^{\mathrm{T}} = \left[0 \;\; 0 \;\; u\left(x, y, t\right) \right]^{\mathrm{T}}. \tag{10}$$

Recalling the governing equation and the linear mechanical theory, the corresponding stresses and strains in the magnetostrictive patch write

$$\sigma_{zx}^{MS} = G^{MS}\left(\varepsilon_{zx}^{MS} - \varepsilon_{ISA}\right), \tag{11}$$

$$\varepsilon_{zx}^{MS} = \frac{1}{2}\frac{\partial u^{MS}}{\partial x}, \tag{12}$$

$$\sigma_{zx}^{h} = G^{h}\varepsilon_{zx}^{h}, \tag{13}$$

$$\varepsilon_{zx}^{h} = \frac{1}{2}\frac{\partial u^{h}}{\partial x}, \tag{14}$$

where superscripts *MS* and *h* stand for the magnetostrictive patch and the host structure, respectively. G^{MS} and G^{h} are the shear modulus of the isotropic piezomagnetic material and that of the host structural metal material, respectively. The equivalent forces generated in the three layers can be obtained from the integral of the thickness of the layers as

$$\tau^{MS} = \int_{t^{MS}} \frac{\partial \sigma_{zx}^{MS}}{\partial x} dy , \tag{15}$$

$$\tau^{h} = \int_{t^{h}} \frac{\partial \sigma_{zx}^{h}}{\partial x} dy , \tag{16}$$

and the pure-shear of the bonding layer yields

$$\tau^{b} = G^{b}\gamma = \frac{G^{b}\left(u^{MS} - u^{h}\right)}{t^{b}}, \tag{17}$$

where G^{b} is the shear modulus of the bonding layer. Parameters t^{MS}, t^{b} and t^{h} denote the thicknesses of the magnetostrictive patch, the bonding layer and the host structure, respectively, as shown in figure 1. Combining Eqs. (12), (14) and the double differentiation of Eq. (17) yields,

$$\varepsilon_{zx}^{MS\prime} = \frac{t^{b}}{G^{b}}\tau^{b\prime\prime} + \varepsilon_{zx}^{h\prime} . \tag{18}$$

The traction free boundary conditions at both vertical surfaces of the patch and bonding layer are given as

$$x = \pm a, \sigma_{zx}^{MS} = \sigma_{zx}^{b} = 0 . \tag{19}$$

Substituting Eqs. (11-14) into Eq. (18) and considering the relationship $\tau^{MS} = \tau^{h} = \tau^{b} = \tau$, one gets the governing equation to solve the interfacial shear stress as,

$$\frac{\partial^{2}\tau}{\partial x^{2}} - \Gamma^{2}\tau = \frac{\partial \varepsilon_{ISA}}{\partial x} . \tag{20}$$

Considering the boundary conditions and substituting the excitation magnetic field H_x into the Eq. (9), and then into Eq. (20), the solution can be written as,

$$\tau = -\frac{G^b}{t^b}\frac{M_0}{k^2+\Gamma^2}\cos(kx), \tag{21}$$

where the parameters M_0, Γ and k are defined as,

$$M_0 = kd_{5x}\frac{2I}{\pi a}\sin\left(\frac{\pi w}{D}\right)e^{-2\pi h/D}e^{qy}, \tag{22}$$

$$\Gamma^2 = \frac{G^b}{t^b t^{MS} G^h}\frac{(\psi+1)}{\psi}, \tag{23}$$

$$k = \frac{\pi}{a}, \tag{24}$$

$$\psi = \frac{t^h G^h}{t^{MS} G^{MS}}, \tag{25}$$

2.3 Wave propagation

The in-plane displacement of the SH0 mode wave in the plate can be assumed as,

$$u_z(x,y,t) = A_0 y e^{i\xi_0^S x}e^{-i\omega t}, \tag{26}$$

where superscript S denotes the symmetric mode and ξ is the wave number in the x direction. To facilitate the model development, the NME framework is introduced to deal with the surface excitation problem [10]. The complex reciprocity and the model orthogonal relation [37] give

$$4P_{nn}\left(\frac{\partial}{\partial x}-i\tilde{\xi}_n\right)a_n(x)-\tilde{\mathbf{v}}_n(d)\cdot\tau(x)=0, \tag{27}$$

with

$$P_{nn}=\frac{1}{4}\int_{-d}^{d}\left[\tilde{\mathbf{v}}_n(y)\cdot\mathbf{T}_n(y)+\mathbf{v}_n(y)\cdot\tilde{\mathbf{T}}_n(y)\right]\cdot\hat{x}dy, \tag{28}$$

where $a_n(x)$ represents the modal participation factor. Here $\mathbf{v}_n$ and $\mathbf{T}_n$ denote the wave velocity and the wave stress, respectively. Substituting Eq. (21) into Eq. (27) gives,

$$a_n(x)=\frac{\tilde{\mathbf{v}}_n(d)}{4P_{nn}}e^{i\tilde{\xi}_n x}\left\{\begin{array}{l}-\dfrac{G^b}{t^b\left(k^2+\Gamma^2\right)}kd_{5x}\dfrac{2I}{\pi a}\sin\left(\dfrac{\pi w}{D}\right)\\ \times\left[\dfrac{1}{ik-i\tilde{\xi}_n}e^{\left(ik-i\tilde{\xi}_n\right)}-\dfrac{1}{ik+i\tilde{\xi}_n}e^{\left(-ik-i\tilde{\xi}_n\right)}\right]\end{array}\right\|_{-a}^{a}. \tag{29}$$

In this work, tone-burst excitations are used. Given a certain position x_0, the frequency response function, $G(\omega)$, can be obtained from Eq. (29). Subjected to an excitation signal $f_e(t)$, the time-domain displacement responses can be obtained as,

$$u(x_0,t)=\mathrm{F}^{-1}\left[\mathrm{F}\left(f_e(t)\right)\cdot G(\omega)\right], \tag{30}$$

where $\mathrm{F}(\square)$ and $\mathrm{F}^{-1}(\square)$ represent the direct and inverse Fourier transform, respectively.

Finally, by combining the three aforementioned modeling blocks, the whole process of SH0 wave generation and propagation by an MsT can be simulated, resulting in the temporal signals of strain or displacement at any position over the plate.

3 Numerical results and analyses

Numerical studies are carried out with a twofold purpose: to validate the proposed theoretical model and to ascertain the designed optimal MsT-activated SHM system with the frequency tuning characteristics. For validation purposes, a 3-D FE model is constructed using *Comsol Multiphysics*, as shown in figure 2. The color map represents the shear stress component σ_{13} to illustrate the generated SH waves in the plate. The length, width and thickness of the host plate are 240, 150, and 2 mm, respectively. The configuration allows for a proper balance between the signal complexity resulting from the boundary reflections and the calculation cost. A MsT patch (50×50 mm) is bonded on the top surface of the host plate through a thin adhesive layer. In addition, infinite elements are applied to the four edges of the plate model and the MsT patch to minimize the wave reflection from the boundaries. The materials of the MsT patch, bonding layer and host plate are iron-cobalt alloy, epoxy and 2024-T3 alloy, respectively. The material parameters of each components used in the simulations are tabulated in table 1. Free quad meshes are used with the mesh size being smaller than 10% of the shortest wavelength of interest. Meanwhile, the sampling frequency is set 20 times the excitation frequency. For consistency, a 12-cycle tone-burst excitation signal modulated by Hann window is used in both theoretical and the FE models, as shown in figure 3(a). The distribution of the excitation magnetic field in the numerical simulations takes the form of H_x as presented in Eq. (6), and the field intensity is set to 1 A/m. It is worth noting that the static magnetic field is not directly simulated in the models but by using a set of carefully selected piezomagnetic coefficients [35]. As a representative case, the meander-line periodicity distance D is set to 10 mm in both the theoretical and FE models.

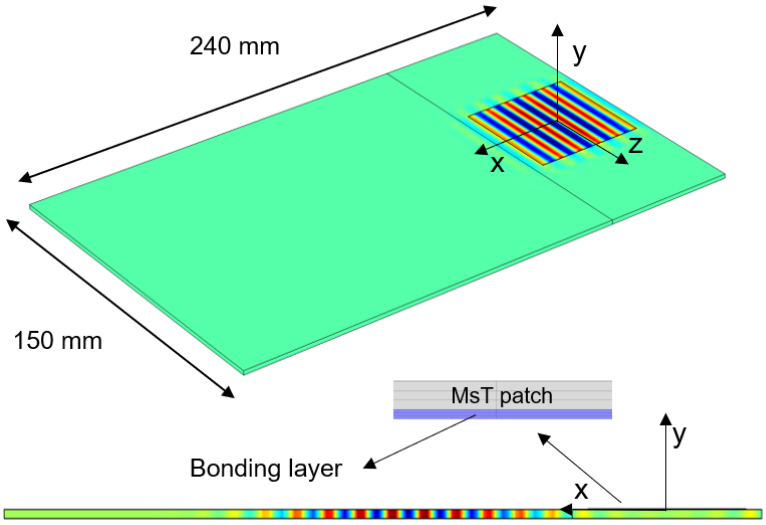

Figure 2. Schematic diagram of the FE model.

Table 1. Parameters used in the theoretical and FE models.

Magnetostrictive material					
Thickness	Density	E	ν	d_{15}	$\bar{\mu}$
0.1 mm	7800 kg/m^3	200 GPa	0.4	1.5e-8 m/A	18000
Bonding layer					
Thickness	Length	Width	Density	E	ν
0.03 mm	50 mm	50 mm	1060 kg/m^3	3.5 GPa	0.33
Aluminium plate					
Thickness	Length	Width	Density	E	ν
2 mm	240 mm	150 mm	2700 kg/m^3	70 GPa	0.33

At first, frequency tuning curves of the SH0 wave signals are calculated with the FE model at the sensing point $x_0 = 180$ mm. Excitation frequency is varied from 50 kHz to 550 kHz with a 5 kHz step. The displacement amplitude of the response at each excitation frequency is extracted. Take 300 kHz case as an example, the 12-cycle excitation signal and the acquired time-domain signal are normalized and depicted in figure 3(a). In order to precisely extract the wave amplitude at different frequencies, complex Morlet wavelet transform is applied to calculate the modulus of the wavelet coefficients, as shown in figure

3(b). Evaluating the arriving time and calculating the group velocity (about 3000 m/s) confirm the SH0 wave mode of the wave packet. Then, the amplitude of the wavelet coefficients at the calculated arriving time of SH0 waves is extracted. By assembling the amplitudes at different frequencies, a frequency tuning curve from the FE simulation can be obtained to further compare with the one calculated from the theoretical model, as shown in figure 4. It follows that, below 370 kHz, both sets of results exhibit a remarkably similar tendency, especially in terms of the positions of the peak and valley points, demonstrating that the dependence of the wave amplitude on the excitation frequencies is well characterized by the theoretical model proposed in this paper. Since the dynamics of the actuator are not considered in the theoretical model, the shear-lag solutions are only valid in the low-frequency range. In addition, in the 3-D FE simulations, the generated SH waves are nonplanar and the wave beam divergence differ at different frequencies. Therefore, the frequency tuning characteristics will, in principle, be affected by the sensing positions in the finite element simulations. Having said that, within the frequency range of interest considered in this study, analyses confirm that the influence of the sensing position is not significant, especially in terms of the positions of peaks and valleys from SHM application perspective. Due to these limitations, the lack of agreement at higher frequencies exceeding 370 kHz is observed and understandable with explanations discussed in a similar but different context [38].

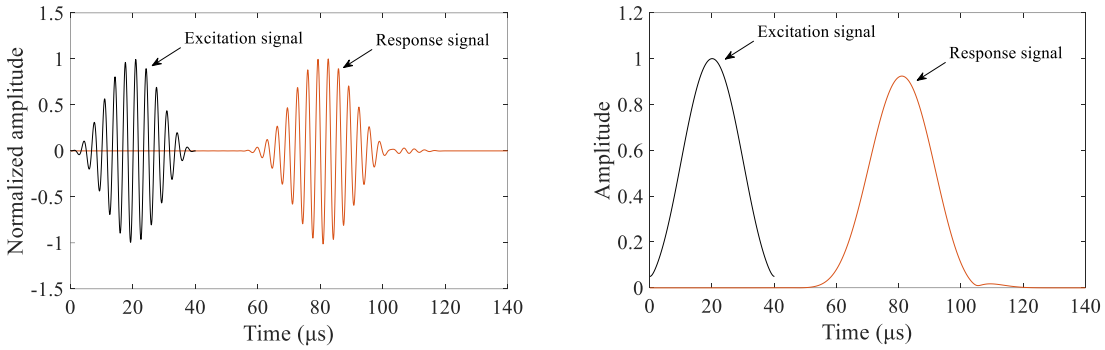

Figure 3. (a) 12-cycle excitation signal with the central frequency at 300 kHz and corresponding time-domain wave response; (b) the modulus of the wavelet coefficients at 300 kHz.

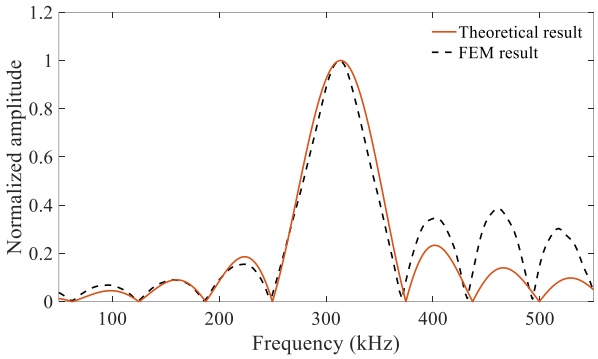

Figure 4. Normalized frequency tuning curves of the SH0 wave mode obtained in the theoretical model and the FE simulations.

To further validate the theoretical model in terms of the temporal, amplitude and phase information, four representative cases are selected with the excitation frequencies at 200 kHz, 250 kHz, 300 kHz and 370 kHz. The SH-wave particle displacements at the sensing point $x_0 = 180$ mm are calculated using the theoretical and the FE models, respectively. Figure 5(a) shows a comparison of the time-domain responses with the excitation central frequency at 200 kHz. It can be clearly seen that the two curves match well. Similar consistency can also be found in figure 5(b) to (d) with different excitation frequencies. As mentioned before, the slight discrepancies between the theoretical and simulation results of the time domain signals in figures 5(b) to (d) are mainly attributed to the limitation of

the shear-lag model, which by nature, is applicable to the low-frequency range investigated in this paper due to the omission of the inertial terms. Nevertheless, as long as the wave propagation and the energy level of the wave signals are correctly predicted, the accuracy of the phase prediction for SHM applications is not critical since the frequency content in a conventional used tone-burst excitation signal is rather narrow. Specifically, when the central frequencies of the excitation signals are around the valleys of the frequency tuning curve (figure 4), calculations using the proposed model and the FEM both reveal a split of the generated SH0 wave packet, as shown in figure 5(b) and (d). A plausible explanation can be made as follows. The sine function excitation signal which is modulated by Hann window has a certain frequency bandwidth near the central frequency. When the central frequency response is inhibited (right at the valley of the of the frequency tuning curve), the side-band responses dominate the signals, as evidenced by the transformed amplitude spectra (FFT results) shown in figure 6 for 250 kHz case. FFT allows one to better discern the tiny differences in the weak energy region between the two main peaks. Generally, the peak region draws more attention in views of obtaining strong SH waves. However, the valley regions are still worthy of study when the elimination of some particular frequencies is required in the SHM applications.

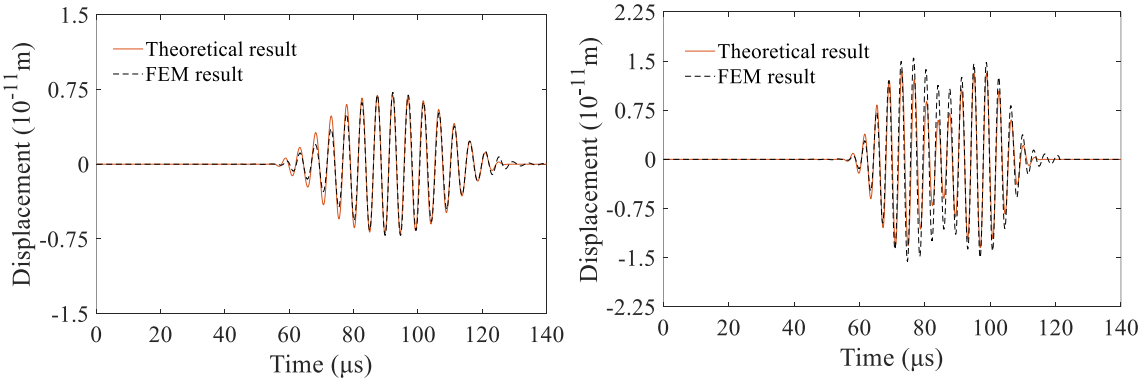

(a) (b)

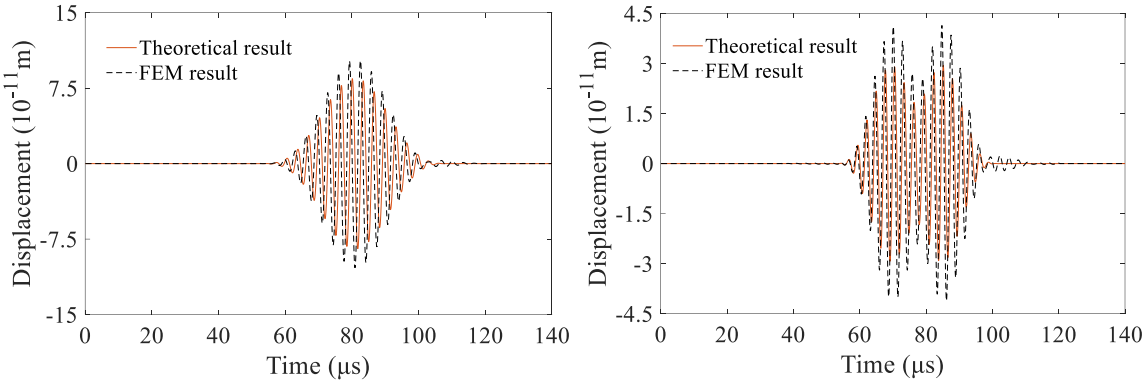

Figure 5. Comparisons of the time-domain responses for the excitation frequency equal to: (a) 200 kHz, (b) 250 kHz, (c) 300 kHz, (d) 370 kHz.

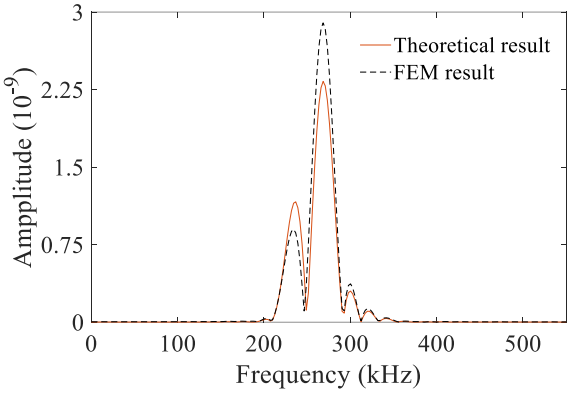

Figure 6. Comparisons of the frequency-domain responses with the excitation central frequency as 250 kHz.

Therefore, the proposed theoretical model, with the consideration of all necessary basic elements and their inter-couplings, shows sufficient accuracy to simulate SH0 wave generation and propagation process and to guide the selection of the excitation frequency as well as other system parameters towards a rational SHM system design.

4 Experimental validation

Experiments are carried out for further validations of the proposed model. The experimental set-up is sketched in figure 7. An aluminum plate of 1000×1000×1 mm was vertically suspended using elastic strings to mimic free boundary conditions. A *PSV-400-3D Scanning Vibrometer* was used to collect wave responses from the surface of the plate [39]. A 300×300 mm retroreflective patch was surface-bonded to increase the intensity of the reflected laser beams and signal-to-noise ratio. An MsT actuator was mounted on the back surface of the plate to avoid any shielding for the measurement of the wave field near the excitation region. A 52×52 mm iron-cobalt-alloy patch was firstly bonded on the surface of the host plate using UHU plus 2-component epoxy adhesive. The length and width of the patch are larger than the area covered by the meander coil. The meander coil was tightly placed above the magnetostrictive patch whose thickness is approximately 0.1 mm. The periodicity distance of the meander-line coil used in the experiments is 10.3 mm. Finally, an 8-T permanent magnet was fixed to provide the static magnetic field. Specifically, an electrical matching network described in [26] is used to ensure the maximum power transmission from the power amplifier to the coil and to reduce the current reflected in the transmission cables.

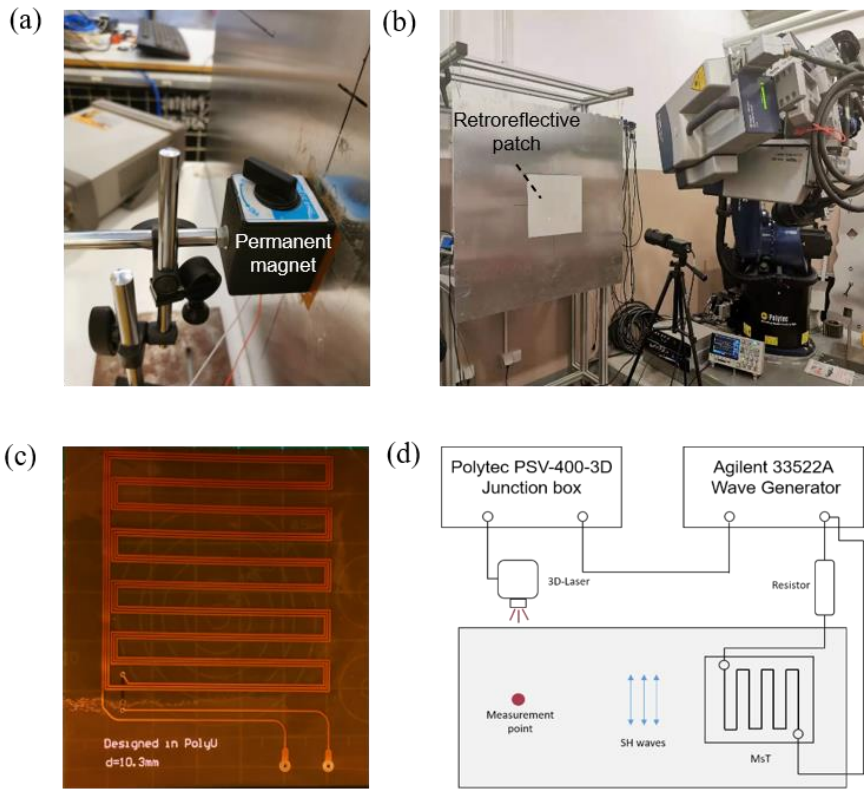

Figure 7. Experimental arrangements: (a) the back of the plate; (b) the front of the plate; (c) sheet coil fabricated by a printed circuit technique (D = 10.3 mm and N_f = 5); (d) schematic of the experimental set-up.

A 12-cycle tone-burst excitation signal with Hann window was used in the tests with a central frequency sweeping up to 400 kHz. Considering the frequency range and the wavelengths of the SH0 mode waves, the mesh size was set to 2 mm, which is dense enough for the wavefield image. The scanned area (200×80 mm) consists of 6426 measurement points. The temporal sampling frequency was 2.5 MHz. For each test, 100 signals were recorded and averaged to reduce the influence of the measurement noise. As a representative case, figure 8(a)-(d) show the x-direction wavefield images in which the dominant signals are identified as the SH waves. In this case, the excitation central frequency is 280 kHz. The position of the MsT transducer, which is marked by a black dash rectangular box in figure 8(a). The results illustrate that the wave packet is generated

by the MsT (figure 8(a)), travels to the upper edge of the plate (figure 8(b) and (c)), and after the reflection from the upper edge, travels back to the bottom of the plate (figure 8(d)).

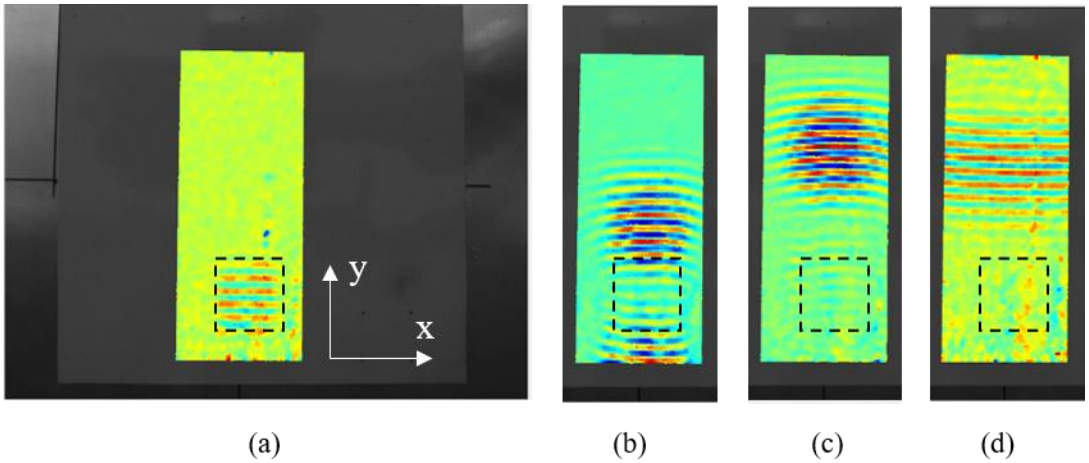

Figure 8. X-direction wave field for the excitation frequency equal to 280 kHz captured after (a) 16.8 μs; (b) 48.83 μs; (c) 71.09 μs and (d) 378.52 μs.

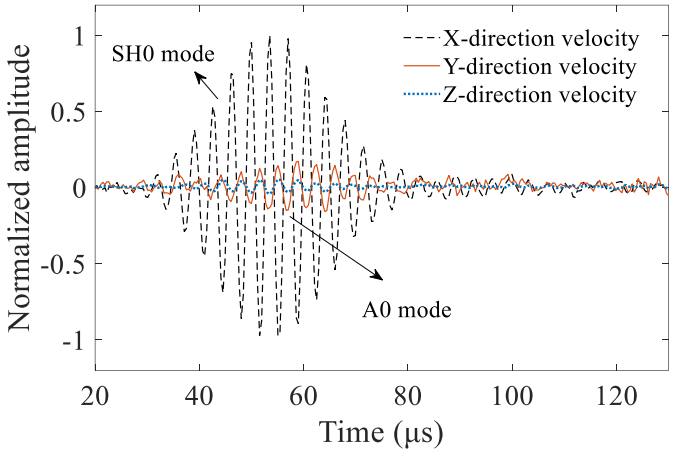

Figure 9. Velocity responses along the three-directions in time domain ($f_0 = 280$ kHz).

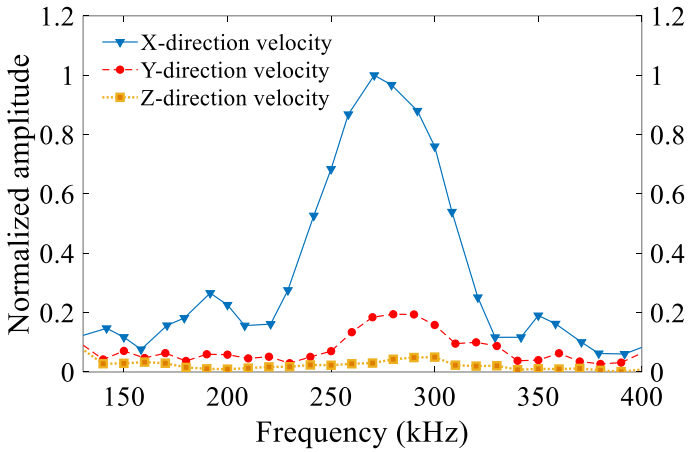

Figure 10. Frequency spectrum of the velocity field in three directions obtained from experimental results.

First, the wave field generated by the MsT is evaluated. The guided waves propagating along *y*-direction were captured when considering the pitch-catch configuration between the MsT and the sensor point. With the help of the 3-D Laser system, the particle oscillations in the three directions were measured in a rectangular coordinate. While the *x*-direction motion was identified to be the SH waves, the *y*- and *z*-direction motions, if exist, are attributed to the Lamb waves in the plate. Figure 9 shows the velocity responses along the three directions at 280 kHz (central frequency of the tone-burst signal) at $x_0 = 100$ mm. The dominant wave packet has been identified to be the SH0 mode wave. Through the calculation of the group velocity, two velocity components at *y*- and *z*-directions are confirmed to correspond to the A0 mode, demonstrating the existence of Lamb waves in the system. Due to the finite size of the permanent magnet and the coil, it was difficult to guarantee that the static and dynamic magnetic fields are precisely perpendicular to each other. Therefore, Lamb wave modes were inevitably generated. A0 waves were observed to be stronger than the S0 waves. It is worth noting that the proposed theoretical model

only considers the pure shear deformation of the magnetostrictive patch, no Lamb wave is obtained in the theoretically predicted results.

Then, the frequency spectra of the three directional oscillations obtained from the experimental results are normalized to the maximum value of the *x*-direction velocities, as shown in figure 10. The responses in the *x*-direction are seen to be more significant than those in the other two directions within the frequency range of interest. This means the Lamb waves generated by the MsT have much smaller amplitudes than the SH waves. Therefore, the components of responses associated to the Lamb waves can be reasonably ignored in the subsequent analyses.

Then, the characteristics of the generated SH waves are assessed using experimental data. As representative cases, the normalized time-domain velocity responses of the SH waves at 220 kHz and 280 kHz, obtained from both the proposed model and experimental measurements are compared in figure 11. The aforementioned wave packet split phenomenon can be observed from both sets of results in figure 11(a). This is predicted by the theoretical model since 220 kHz is located around the valley region of the frequency tuning curve. As for the peak region excitation, a single dominant wave packet obtained from the theoretical model is validated by the experiment, as shown in figure 11(b). As mentioned before, the slight mismatching of the wave phase is mainly attributed to the limitation of the shear-lag model in terms of the omission of low-frequency-specific inertial terms. As pointed out earlier, a perfect wave phase prediction is not pursued for SHM applications. Hereby, the predicated results shown in figure 11(b) are deemed consistent with the theoretical results and acceptable from SHM perspective.

Finally, the frequency tuning curves are compared to further validate the theoretical model in the perspective of wave amplitude prediction, as shown in figure 12. The amplitude of the SH waves reaches the maximum at around 275 kHz in the experiment, in agreement with the theoretical prediction. In the extremely low frequency region, near-field effect may contribute to some noticeable discrepancies. As for the high frequency region, the differences are mainly due to the same limitation of the shear-lag model discussed previously. Nevertheless, the developed theoretical model allows accurate prediction of the frequency tunning characteristics around the targeted design frequency range of the coil where the amplitude is large, which is more relevant to SHM applications.

In summary, some vital SHM promising characteristics, such as the frequencies to generate the maximum and minimum wave amplitude, and the general variation of the frequency tuning curves predicted by the theoretical model, are validated by experimental results. The theoretical model can provide the necessary temporal, phase, and amplitude information to guide the SHM design.

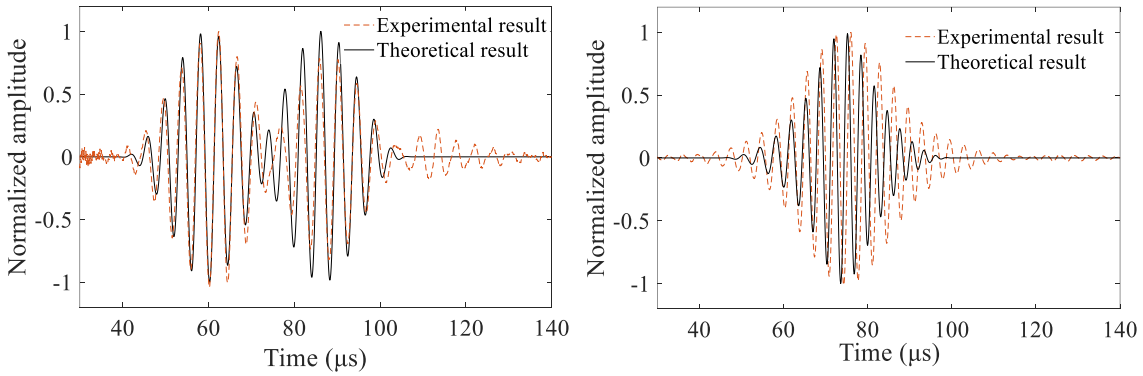

(a) $f_0 = 220$ kHz (b) $f_0 = 280$ kHz

Figure 11. Comparison of time-domain responses between theoretical model and experimental model.

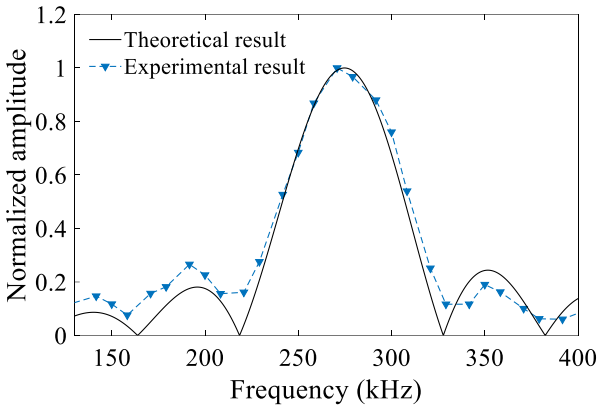

Figure 12. Comparison of frequency tuning curves obtained from experiments (with matching networks) and theoretical model.

5 Guidance for MsT system design

The proposed model is further used to investigate the effects of some key parameters involved in the design of the MsT to eventually achieve better system performance in terms of strong SH0 wave generation. Specifically, the coil configuration and the bonding conditions of MsTs are considered as they can be flexibly tuned.

5.1 Influence of the coil configuration

Two major parameters, i.e., the periodicity distance D of the coil and its fold number N_f are considered. At first, D is tuned to illustrate its effect on the frequency tuning curves. With the material properties tabulated in table 1, the frequency tuning curves corresponding to D = 10, 5 and 3.3 mm are shown in figure 13(a). For the first case, the maximum SH0 wave amplitude is achieved at 312 kHz, consistent with figure 4 as expected. The optimal frequency for the maximum SH0 wave generation obviously increases when D decreases, along with a reduction in its maximum amplitude and an enlargement of the bandwidth, typical of system behavior due to frequency increases. Furthermore, by calculating the corresponding wavelength of the SH0 waves for the three optimal frequencies (9.96, 4.96

and 3.28 mm respectively for the 10-, 5- and 3.3-mm coils), an obvious matching between the spatial period of the coil and the wavelength is observed.

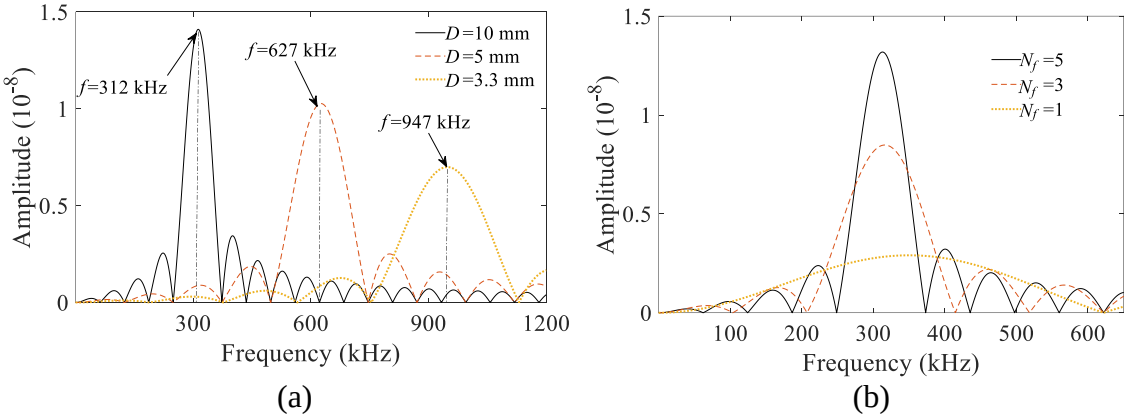

Figure 13. Variation of the frequency tuning curves with respect to different (a) spatial periods of the coil; (b) fold numbers of the coil.

Alongside figure 13(a), the influence of the fold number of the coil N_f is shown. Setting D = 10 mm, three cases with N_f = 5, 3 and 1 are considered, giving the corresponding frequency tuning curves in figure 13(b). It can be seen that the number of the peak and valley points, as well as the maximum magnitude, increases with N_f, as a result of the increasing wave energy enhancement coil after coil. To better show the influence of the N_f, time-domain responses is further investigated by considering its correlation with the cycles of excitation signals N_c. At 300 kHz and D = 10 mm, which closely satisfy the matching condition for the optimal SH0 wave generation, the time-domain SH0 responses to different N_f and N_c are examined. A typical example with and different N_c is shown in figure 14(a). A larger N_c leads to a significant increase in the wave amplitude due to the enhanced energy accumulation within the activation area. By extracting the maximum amplitudes for different N_f and N_c, the correlation between the two parameters can be visualized in figure 14(b). For the 1-fold coil, the amplitude of the SH0 waves is rather

insensitive to the excitation cycle. Further increasing N_f amplifies the signal strength at an increasing rate before asymptotically converge to a stable value, which is different for different N_f. This suggests two important pieces of information which are useful for system design: 1) increasing the fold number and the wave excitation cycles would increase the energy level of the generated SH0 waves; 2) in addition to the spatial matching between the periodicity distance of the coil and the targeted wavelength, the fold number and wave excitation cycles should also be matched to ensure a high wave generation efficiency.

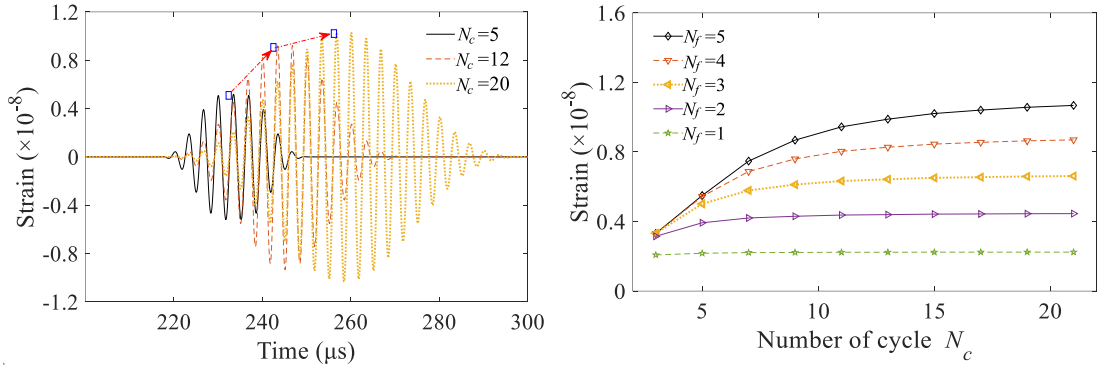

Figure 14. (a) Comparison of theoretical results for the excitation signals with N_c = 5,12 and 20 when f_0 = 300 kHz and N_f = 5; (b) the curves of the maximum signal amplitudes with the changes of excitation signal cycle number.

5.2 Influence of the bonding conditions

Bonded on the host plate, the bonding quality of MsT patches and its influence on the wave generation efficiency are examined. The proposed model, Eq. (21), shows that the influence of the bonding mainly depends on its shear modules and thickness. They are combined as an interface parameter, $\mathrm{K} = G^b/t^b$ in the subsequent analyses. The extreme case of a perfect bonding with $\mathrm{K} = \infty$ is compared with a practical bonding case with K = 1.5×10^{13} N/m^3 (taken from our measurements with the G^b = 0.45 GPa and t^b = 0.03 mm).

Using D = 5 mm and N_f = 5 in both cases, the corresponding frequency tuning curves are compared in figure 15(a). It can be seen that the bonding condition mainly affects the amplitude of the generated SH0 wave instead of the position of the optimal frequency, which is understandable from the discussions in the previous section. To further quantify this, the influence of the bonding conditions on the generated optimal SH wave amplitudes for different periodicity distance of coils is discussed. In practice, the bonding thickness should affect K more than the shear modulus does since the former has a much larger variation range (5 μm to 100 μm as described in [31]). Therefore, considering the minor variation of shear modulus at around 0.5 GPa and the above-mentioned thickness range, K is varied between 1×10^{13} N/m^3 and 10×10^{13} N/m^3 to represent a realistic variation range. An even larger K would approach a nearly perfect bonding case. The generated optimal SH wave amplitudes for the three coil configurations are then extracted and compared in figure 15(b). For different D values, the corresponding maximum amplitudes appear at different frequencies (f_{max}=312 kHz for D=10 mm; f_{max}=627 kHz for D=5 mm; f_{max}=947 kHz for D=3.3 mm). It can be seen that, in the realistic bonding region, bonding conditions affect the wave generation more significantly for a smaller periodicity period of the coil, as evidenced by the steepness of the curves. For the same level of excitation and approaching the perfect bonding conditions with an extremely large K, the maximum SH0 wave amplitudes would be getting close, but discrepant at these corresponding frequencies.

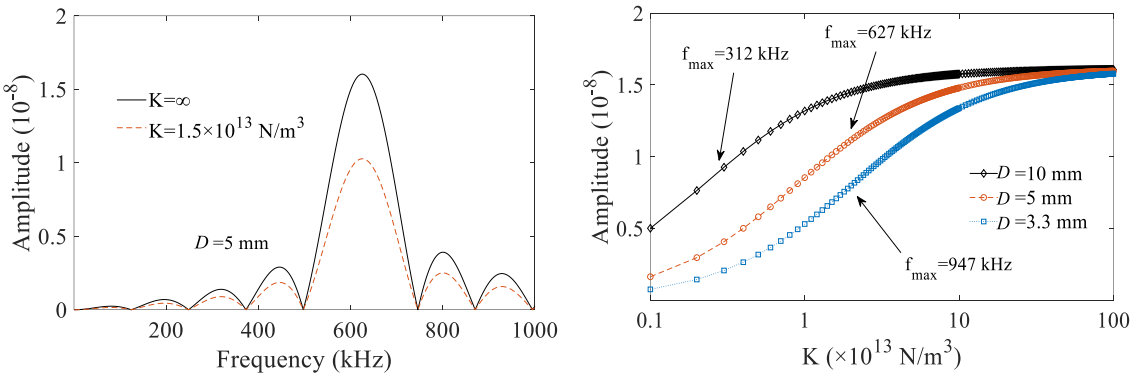

Figure 15. (a) Frequency tuning curves of realistic bonding and perfect bonding conditions; (b) variation of maximum amplitudes extracted from the frequency tuning curves against interface parameter K.

The above findings can be further used to guide the design of the MsT-based SHM systems. Some remarks would help better understand the context of the study and possible utilization of the model when more realistic factors need to be considered. Alongside the coil configuration and the bonding conditions, the configurations of MsT patch might also affect, but presumably to a less extent, the SH wave generation. First, the room to tune the patch thickness in practical SHM applications is very limited with the concern of limiting its effects on the structure under inspection. This can certainly be further assessed when a thickness variation range is defined. Second, as to the size of the patch, it is known that it is the area under the coil that is mainly responsible for the SH wave generation. This so-called effective area is modeled in the present work, and its influence has been investigated in the paper by changing the number of the coil and the special periodic distance. In practical implementation where the actual patch size might be slightly larger than the effective area covered by the coil, the mechanical effect of the exceeding part (outside the effective coil area), is deemed negligible due to the thin thickness of the MsT patch. Third, the bias magnetic field is applied perpendicularly to the dynamic field to enforce the

Wiedemann effect for the generation of shear deformation. The strength of the bias effect will only affect the magnetostriction strength as reflected by the piezomagnetic coefficients, which involve all properties of the magnetostrictive material. Despite its obvious influence on the generated SH wave amplitude, the frequency tuning characteristics of the system, in terms of variation with respect to frequencies, are not affected by this parameter. Finally, the temperature inevitably has certain influence on the system performance in terms of SH wave generation. However, under the normal operation condition, its influence is very limited, thus not being considered in this work.

6 Conclusions

This paper proposes a theoretical model for the prediction of SH0 wave generation and propagation, activated by a MsT in an aluminum plate. The coupling of the electromagnetic and elastic fields, including the adhesive layer, are considered. Specifically, the mechanical coupling between the magnetostrictive patch and the host structure is achieved by the stress transmitting through a thin bonding layer, of which the thickness and shear modulus are considered. The shear-lag model and the NME method are strategically introduced and applied to solve the SH0 wave generation and propagation problem. Validations in terms of both time domain and frequency domain responses are carefully carried out in a wide frequency range through both FE simulations and experimental investigations. It is worth noting that, the system resonance is not considered in this work because the frequency range that under investigation is much lower than the resonance frequency, which should be avoided in SHM applications. Finally, with the proposed theoretical model, the characteristics of coil and bonding layer, and their effects on the generated SH0 wave at both the time domain and frequency domain are systematically investigated.

Results predicted by the proposed model are in good agreement with both FE and experimental results in terms of the temporal and amplitude features of the generated SH0 waves at both the peak and valley regions of the frequency tuning curve. Additionally, the responses obtained from the experiments show that an A0 Lamb wave mode of very small amplitude was also generated by the MsT. Through the selection of the central excitation frequency, however, a relatively pure SH wave packet can be technically generated and captured. The parametric analyses show that the SH0 wave generation is highly related to the coil configuration and bonding conditions, thus providing the essential guidelines for the MsT system design to increase the amplitude and signal-to-noise ratio of the desired mode wave in the plate.

More specifically, the spatial periodicity distance D and the fold number N_f of the coil can significantly affect the frequency tuning characteristics of a MsT system. For a given D, a larger coil fold number within the permissible activation space is always desirable. Meanwhile, the tone-burst excitation cycles should be sufficiently large to further enhance the magnitude of the generated SH0 waves. Above all, the excitation cycles and the fold number of the coil should be matched to guarantee a high wave generation efficiency. As for the bonding conditions, the shear modulus and the thickness of the bonding layer have no influence on the position of the optimal excitation frequency. However, they affect the energy level of the generated SH0 waves. In practical applications, a thin and stiff bonding layer is always preferred for strong wave generation. In addition, a larger periodicity distance of the coil with lower excitation frequency is more robust to the variation of the bonding conditions due to operational or environmental uncertainties. This of course would come with a penalty in the increase of the activation area.

As a final remark, the present model offers a unified platform for physical mechanism exploration, structural design and eventually system optimization for SH0 wave based SHM applications. The developed approach allows fast and easy parametric studies if required. In future work, the limitation of the proposed model in terms of high frequency response prediction should be addressed. Combining the frequency tuning characteristics of both SH waves and Lamb waves, the present model also paves the way forward to the nonlinear SH-wave-based SHM applications for the incipient damage detection.

Acknowledgements

The project was supported by grants from the Research Grants Council of Hong Kong Special Administrative Region (PolyU 152070/16E), the National Natural Science Foundations of China through SHENG project (Polish-Chinese Funding Initiative, 51961135302), Research Fund of State Key Laboratory of Mechanics and Control of Mechanical Structures（Nanjing University of Aeronautics and astronautics, Grant No. MCMS-E-0520K01）and the Innovation and Technology Commission of the HKSAR Government to the Hong Kong Branch of National Rail Transit Electrification and Automation Engineering Technology Research Center. The authors would like to acknowledge Mr. Mariusz Osika from AGH University of Science and Technology for the technical help with the experiment set-up. The authors also would like to acknowledge Prof. Zhifeng Tang from Zhejiang University for providing us with the iron-cobalt foil made by his group.

Declaration of conflicting interests

The author(s) declared no potential conflicts of interest with respect to the research, authorship, and/or publication of this article.

References

[1] Giurgiutiu V 2014 *Structural Health Monitoring with Piezoelectric Wafer Active Sensors* 2nd ed (New York: Academic)

[2] Li P, Shan S, Wen F and Cheng L 2019 A fully-coupled dynamic model for the fundamental shear horizontal wave generation in a PZT activated SHM system *Mech. Syst. Signal Process* **116** 916-932

[3] Shen Y and Cesnik C E S 2018 Local Interaction Simulation Approach for Efficient Modeling of Linear and Nonlinear Ultrasonic Guided Wave Active Sensing of Complex Structures *J. Nondestruct. Eval., Diagn. & Progn. Eng. Syst.* **1** 011008

[4] Fortunko C M, King R B and Tan M 1982 Nondestructive evaluation of planar defects in plates using low-frequency shear horizontal waves *Int. J. Appl. Phys.* **53**(5) 3450-3458

[5] Rose J L, Pelts S P and Li J 2000 Quantitative guided wave NDE *15th World Conf. NDT (Rome)*

[6] Su Z, Yang C, Pan N, Ye L and Zhou L M 2007 Assessment of delamination in composite beams using shear horizontal (SH) wave mode *Compos Sci Technol* **67**(2) 244-251

[7] Zhou W, Li H and Yuan F G 2015 Fundamental understanding of wave generation and reception using d36 type piezoelectric transducers *Ultrasonics* **57** 135-143

[8] Kim Y Y and Kwoon Y E 2015 Review of magnetostrictive patch transducers and applications in ultrasonic nondestructive testing of waveguides *Ultrasonics* **62** 3-19

[9] Belanger P and Boivin G 2016 Development of a low frequency omnidirectional piezoelectric shear horizontal wave transducer *Smart Mater. Struct.* **25**(4) 045024

[10] Kamal A and Giurgiutiu V 2014 Shear horizontal wave excitation and reception with shear horizontal piezoelectric wafer active sensor (SH-PWAS) *Smart Mater. Struct.* **23**(8) 085019

[11] Harish A V, Ray P, Rajagopal P, Balasubramaniam K and Srinivasan B 2016 Detection of fundamental shear horizontal mode in plates using fibre Bragg gratings *J. Intell. Mater. Syst. Struct.* **27**(16) 2229-2236

[12] Miao H, Huan Q, Wang Q and Li F 2017 A new omnidirectional shear horizontal wave transducer using face-shear (d24) piezoelectric ring array *Ultrasonics* **74** 167-173

[13] Miao H, Huan Q and Li F 2016 Excitation and reception of pure shear horizontal waves by using face-shear d24 mode piezoelectric wafers *Smart Mater. Struct.* **25**(11) 11LT01

[14] Miao H, Dong S and Li F 2016 Excitation of fundamental shear horizontal wave by using face-shear (d36) piezoelectric ceramics *Int. J. Appl. Phys.* **119**(17) 174101

[15] Zhou W, Li H and Yuan F G 2013 Guided wave generation, sensing and damage detection using in-plane shear piezoelectric wafers *Smart Mater. Struct.* **23**(1) 015014

[16] Rouge C, Lhémery A and Ségur D 2012 Modal solutions for SH guided waves radiated by an EMAT in a ferromagnetic plate *J. Phys: Conference Series* **353**(1) 012014

[17] Calkins F T, Flatau A B and Dapino M J 2007 Overview of magnetostrictive sensor technology *J. Intell. Mater. Syst. Struct.* **18**(10) 1057-1066

[18] Lissenden C J, Liu Y, Choi G W and Yao X 2014 Effect of localized microstructure evolution on higher harmonic generation of guided waves *J. Nondestruct. Eval.* **33**(2) 178-186

[19] Kwun H and Bartels K A 1998 Magnetostrictive sensor technology and its applications *Ultrasonics* **36** 171-178

[20] Shan S, Hasanian M, Cho H, Lissenden C J and Cheng L 2019 New nonlinear ultrasonic method for material characterization: Codirectional shear horizontal guided wave mixing in plate *Ultrasonics* **96** 64-74

[21] Shan S and Cheng L 2019 Mixed third harmonic shear horizontal wave generation: interaction between primary shear horizontal wave and second harmonic Lamb wave *Smart Mater. Struct.* **28**(8) 085042

[22] Thompson R B 1973 A model for the electromagnetic generation and detection of Rayleigh and Lamb waves *IEEE T Ultrason Free* **20**(4) 340-346

[23] Thompson R B 1990 Physical principles of measurements with EMAT transducers *Phys. Acoust.* **19** 157-200

[24] Ogi H, Hirao M and Minoura K 1997 Noncontact measurement of ultrasonic attenuation during rotating fatigue test of steel *Int. J. Appl. Phys.* **81**(8) 3677-3684

[25] Ogi H 1997 Field dependence of coupling efficiency between electromagnetic field and ultrasonic bulk waves *Int. J. Appl. Phys.* **82**(8) 3940-3949

[26] Huang S, Wang S, Li W and Wang Q 2016 *Electromagnetic ultrasonic guided waves* Springer Singapore

[27] Cho S H, Lee J S and Kim Y Y 2006 Guided wave transduction experiment using a circular magnetostrictive patch and a figure-of-eight coil in nonferromagnetic plates *Appl. Phys. Lett.* 88(22) 224101

[28] Liu Z, Zhang Y, Xie M, Li A, Bin W and He C 2018 A direction-tunable shear horizontal mode array magnetostrictive patch transducer *NDT E Int* 97 20-31

[29] Wu J, Tang Z, Yang K and Lv F 2019 Signal strength enhancement of magnetostrictive patch transducers for guided wave inspection by magnetic circuit optimization *Appl. Sci.* 9(7) 1477

[30] Kim H J, Lee J S, Kim H W, Lee H S and Kim Y Y 2014 Numerical simulation of guided waves using equivalent source model of magnetostrictive patch transducers *Smart Mater. Struct.* 24(1) 015006

[31] Shan S, Wen F and Cheng L 2017 Mitigation of Adhesive Nonlinearity in Nonlinear-Lamb-wave-based SHM Systems *Struct. Health Monit. 2017*

[32] Giurgiutiu V 2005 Tuned Lamb wave excitation and detection with piezoelectric wafer active sensors for structural health monitoring *J. Intell. Mater. Syst. Struct.* **16**(4) 291-305

[33] Hirao M and Ogi H 2017 *Electromagnetic acoustic transducers* Tokyo, Japan Springer

[34] Ogi H, Goda E and Hirao M 2003 Increase of efficiency of magnetostriction SH-wave electromagnetic acoustic transducer by angled bias field: Piezomagnetic theory and measurement *Int. J. Appl. Phys.* **42**(5S) 3020

[35] Nye J F 1957 *Physical Properties of Crystals* Oxford University. Press (clarendon) London

[36] Engdahl G and Mayergoyz I D 2000 *Handbook of giant magnetostrictive materials* San Diego: Academic press

[37] Shan S, Cheng L and Wen F 2018 Design of nonlinear-Lamb-wave-based structural health monitoring systems with mitigated adhesive nonlinearity *Smart Mater. Struct.* **27**(10) 105006

[38] Dugnani R 2016 Extension of the Crawley's adhesive model to dynamically actuated piezoelectric transducers *J. Intell. Mater. Syst. Struct.* **27**(15) 2112-2124

[39] Leong W H, Staszewski W J, Lee B C and Scarpa F 2005 Structural health monitoring using scanning laser vibrometry: III. Lamb waves for fatigue crack detection *Smart Mater. Struct.* **14** 1387-1395